AIP | Journal of Applied Physics

Time- and vector-resolved magneto-optical Kerr effect measurements of large angle precessional reorientation in a 2×2μm2 ferromagnet

P. S. Keatley, V. V. Kruglyak, A. Neudert, M. Delchini, R. J. Hicken et al.

Citation: J. Appl. Phys. **105**, 07D308 (2009); doi: 10.1063/1.3056405
View online: http://dx.doi.org/10.1063/1.3056405
View Table of Contents: http://jap.aip.org/resource/1/JAPIAU/v105/i7
Published by the American Institute of Physics.

Time- and vector-resolved magneto-optical Kerr effect measurements of large angle precessional reorientation in a 2×2 μm^2 ferromagnet

P. S. Keatley,[1,a] V. V. Kruglyak,[1] A. Neudert,[1] M. Delchini,[1] R. J. Hicken,[1] J. R. Childress,[2] and J. A. Katine[2]
[1]*School of Physics, University of Exeter, Exeter, Devon EX4 4QL United Kingdom*
[2]*Hitachi Global Storage Technologies, San Jose Research Center, San Jose, California 95135, USA*

(Presented 11 November 2008; received 17 September 2008; accepted 15 October 2008; published online 18 February 2009)

The precessional dynamics of a 2×2 μm^2 CoFe/NiFe (4.6 nm) element stimulated by an in-plane pulsed magnetic field have been investigated using time- and vector-resolved Kerr microscopy measurements and micromagnetic simulations. The time-resolved signals were normalized to in-plane hysteresis loops obtained from the patterned material, and suggest that the magnetization reorients through an angle of $100° \pm 10°$. The simulations reveal that only the magnetization of the center region undergoes large angle reorientation, while the canted magnetization at the edges of the element remains pinned. An enhanced Gilbert damping parameter of 0.1 was required to reproduce the experimentally observed Kerr signals. © *2009 American Institute of Physics*.
[DOI: 10.1063/1.3056405]

The large angle precessional magnetization dynamics of ferromagnetic elements are expected to underpin the future operation of high frequency magnetic devices, particularly where switching between bistable states is needed or where large angle deflections are required in magnetoresistive sensors. The small amplitude dynamics of microscale elements are governed primarily by dipolar interactions so that the uniformity of the dynamic response is dependent upon the aspect ratio of the element.[1] Recently a number of time-resolved studies of large amplitude dynamics have been performed on thin films and microscale elements.[2–7] In most cases a small value of the static applied magnetic field (bias field) is used so that a large angle deflection may be induced with a pulsed field of modest strength. However, in these circumstances the demagnetizing field makes a significant contribution to the total effective field within the element and a nonuniform ground state magnetization is obtained in elements of nonellipsoidal shape. The effect of this nonuniformity upon the large angle dynamics has not been extensively explored. In this work we study the large angle magnetization dynamics of a 2×2 μm^2 CoFe/NiFe (4.6 nm) element at low bias fields using time-resolved (TR) Kerr microscopy and compare our experimental results with those obtained from micromagnetic simulations. Reasonable agreement was obtained between experiment and simulation by assuming an enhanced value of the Gilbert damping constant.

The 2 μm square element was patterned from a continuous film of nominal composition of Ta(50 Å)/Cu(20 Å)/$Co_{50}Fe_{50}$(7 Å)/$Ni_{92}Fe_8$(45 Å)/Cu(20 Å)/Ru(20 Å)/Ta(20 Å) using e-beam lithography and ion-beam milling. Interdiffusion of the Cu into the magnetic films led to a reduced effective magnetic thickness. From magnetometry measurements on a codeposited continuous film, the effective thickness was found to be 4.6 nm. The element was fabricated upon the 4 μm wide center conductor of a coplanar waveguide (CPW), which was used to deliver a pulsed magnetic field $H_p(t)$ to the element and induce magnetization dynamics (Fig. 1). The magnetization dynamics were measured at a wavelength of 800 nm using a scanning Kerr microscope equipped with a quadrant-photodiode polarizing bridge detector, used to simultaneously detect three components of the vector magnetization, as described in Ref. 8. TR Kerr signals were acquired by using an optical delay line to change the temporal delay of the optical pulse with respect to the pulsed magnetic field. The pulsed field amplitude was modulated at 1.3 kHz to facilitate phase sensitive detection of the Kerr signals.

A bias magnetic field H_b was applied in the plane of the sample and parallel to the CPW. The sample magnetization

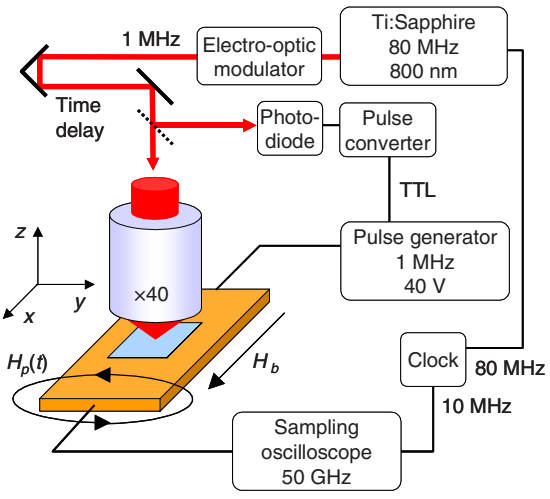

FIG. 1. (Color online) The time-resolved scanning Kerr microscope setup for measurements of large angle magnetization dynamics. The Kerr microscope is equipped with a quadrant photodiode polarizing bridge detector (not shown) that allows three orthogonal components of the vector magnetization to be detected simultaneously.

[a]Electronic mail: p.s.keatley@ex.ac.uk.

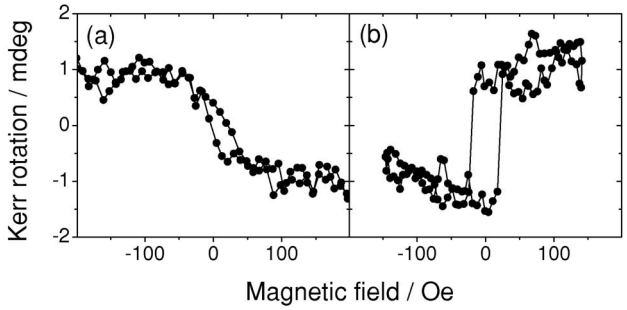

FIG. 2. Hysteresis loops are shown for a 10 μm square element patterned from the same wafer as the 2 μm square element. In (a) and (b) the magnetic field was applied parallel and perpendicular to the coplanar waveguide, respectively.

was saturated in a field of 1 kOe, which was then reduced to 50 Oe. Figure 2 shows focused Kerr hysteresis loops acquired from a 10 μm square fabricated from the same wafer. The loops reveal a uniaxial anisotropy with easy axis approximately perpendicular to the CPW.

TR measurements of small angle precession in a codeposited 10 μm disk were carried out for different orientations and magnitudes of the bias field in order to characterize its magnetic parameters. Figure 3(a) shows a typical TR polar Kerr signal measured with a bias field of 200 Oe applied parallel to the CPW. The dependence of the frequency upon the orientation of the bias field is shown in Fig. 3(b) for a bias field of 300 Oe. In Fig. 3(c) the dependence of the frequency upon the bias field strength is shown when the field was applied parallel to the CPW. The dependence of the frequency upon the field strength and orientation was fitted simultaneously using a macrospin model in which quasialignment of the magnetization and bias field was assumed. Polar Kerr hysteresis loops acquired from the continuous film revealed an effective demagnetizing field of 6.7 kOe corresponding to an effective magnetization of 533 emu/cm^3, while magnetometry measurements on the same films revealed a saturation magnetization of 760 emu/cm^3. The reduced effective magnetization was attributed to surface anisotropy. The uniaxial and surface anisotropy constants were extracted from the fittings and found to be 16300 erg/cm^3 and 0.254 erg/cm^2, respectively. The g-factor was assumed to be 2.1. The easy axis was found to be canted 78° from the length of the CPW in agreement with the focused hysteresis loop measurements.

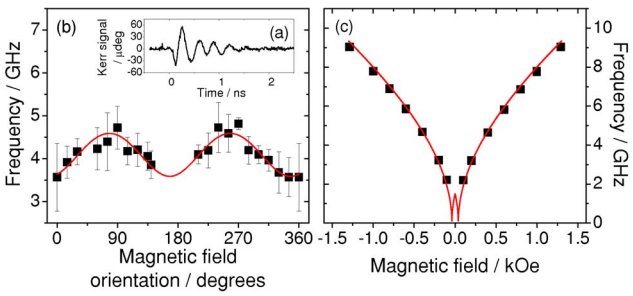

FIG. 3. (Color online) A typical time-resolved Kerr signal of small angle magnetization dynamics in the 10 μm disk is shown in (a). The frequency dependence of the small angle precession is shown for the bias field orientation in (b) and the bias field strength in (c).

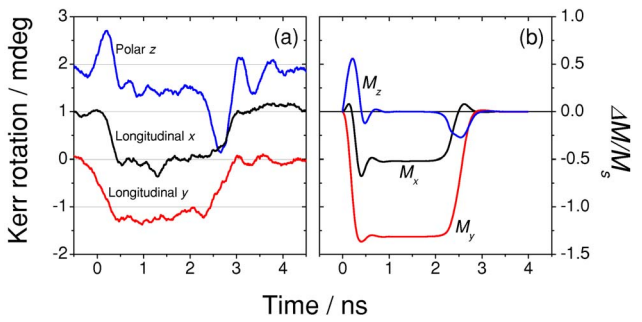

FIG. 4. (Color online) Time-resolved Kerr signals of large angle magnetization dynamics in the 2 μm square element are shown in (a). The longitudinal x and y Kerr signals are proportional to two orthogonal in-plane components of the magnetization that are parallel and perpendicular to the bias field, respectively. The polar Kerr signal is proportional to the out-of-plane component of the magnetization. Simulated traces of the dynamics are shown in (b). The traces are the average response of a region at the center of the element with an area similar to that of the focused laser beam in the scanning Kerr microscope. The $z-$component has be scaled by a factor of 10 for clarity.

Large angle magnetization dynamics were measured for the 2 μm square using the configuration shown in Fig. 1. A pulse generator was used to generate pulses of 35 V amplitude, 2 ns duration, and 150 ps rise time, which were then transmitted through the CPW. The pulse repetition rate was 1 MHz. The pulse generator was connected to the CPW using 50 Ω impedance matched microwave probes. The transmitted voltage amplitude was found to be 3 V using a 50 GHz sampling oscilloscope. Significant attenuation of the pulse occurs due to resistive loss in the CPW. The values of the current and voltage at the position of the sample were estimated to be 0.215 A and 10.75 V, respectively, assuming an exponential decrease of the pulse along the CPW. By integrating the Biot–Savart law over a strip of uniform current density, the amplitude of the pulsed magnetic field was estimated to be 59 Oe. The repetition rate of the laser beam was reduced to 1 MHz using an electro-optic modulator in order to match the repetition rate of the pulse generator. A fast-photodiode signal, generated by the 1 MHz beam, was converted into a transistor-transistor logic (TTL) pulse and then used to trigger the pulse generator so that the electronic pump and optical probe were synchronized.

Figure 4(a) shows TR signals of large angle reorientation measured simultaneously for three components of the vector magnetization. The signals have been smoothed to minimize high frequency noise with a cut-off frequency of ~4 GHz. TR measurements of small angle precession do not show any magnetization dynamics with frequency greater than 2 GHz at a bias field of 50 Oe. Since the in-plane saturation Kerr rotation can be determined from the focused in-plane hysteresis loops, the angle of reorientation can be determined. From Fig. 2 the saturation Kerr rotation is ~1 mdeg. In Fig. 4 the change in the x- and y-axis longitudinal Kerr signal is ~1 and ~1.3 mdeg, respectively. A change in TR Kerr signal of 1 mdeg suggests a rotation through 90°. The change in the y-axis Kerr rotation is larger than the saturation Kerr rotation, suggesting that the static magnetization was initially rotated by a small angle from the x-axis in the opposite direction to the pulsed field. Some rotation from the x-axis is

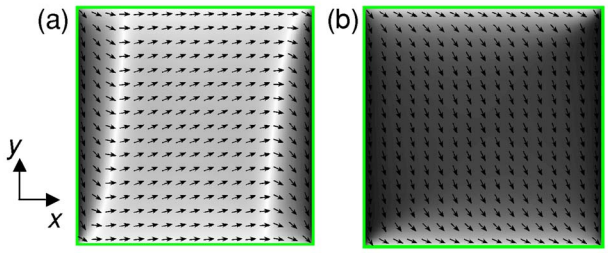

FIG. 5. (Color online) Images of the magnetization are shown at time equal to 0 and 1.5 ns in (a) and (b), respectively. The grayscale represents the *y*-component of the magnetization where black and white corresponds to $\pm M_S$ and $M_y=0$, respectively.

expected since the easy direction of magnetization is 78° from the *x*-axis. Since the angle of rotation is small, the *x*-axis Kerr component was assumed to be saturated. The angle of reorientation was then found to be $100° \pm 10°$.

Micromagnetic simulations were performed using the Object Oriented MicroMagnetic Framework (Ref. 9) for a 2 μm square of thickness of 4.6 nm. A cell size of $10 \times 10 \times 4.6$ nm^3 was used in addition to values given earlier for the saturation magnetization and uniaxial and surface anisotropies. Before dynamic simulations were performed, the magnetization was relaxed (in 100 Oe field steps) from a uniform state to a field of 100 Oe before finally being relaxed in a field of 50 Oe. The Gilbert damping parameter was set to 0.5 in order to accelerate the process. Initially an unstable ground state was obtained. Following the simulated pulsed field excitation, the element acquired a different ground state. Since the TR measurements are stroboscopic, it is unlikely that the initial ground state corresponded to that of the experiments. Therefore we instead assumed the more robust ground state, shown in Fig. 5(a), obtained after the simulated pulsed field excitation. This ground state was used for the dynamic simulations presented in this paper.

In the dynamic simulations, an in-plane pulsed magnetic field was applied in the -*y*-direction. The dynamic simulations were performed over 4 ns in 20 ps time steps. At each time step a vector field map of the components of the vector magnetization was recorded, and the average response of the magnetization components was extracted from an area at the center of the element that was similar to that of the focused optical probe used in the experiments. The response at each time step was then compiled to generate the TR traces for each magnetization component shown in Fig. 4(b). In order to reproduce the experimental Kerr signals it was necessary to use a Gilbert damping parameter of 0.1. Qualitatively, the simulated traces are in reasonable agreement with the experimental Kerr signals. In Figs. 4(a) and 4(b), the traces for the *x*-component lag the *y*-component following the pulsed field excitation. The maximum change in the *x*-component is also found to be less than that for the *y*-component, although to a lesser extent in the experimental Kerr signals. Finally both experimental and simulated *z*-components show precession of opposite phase during the rise and fall of the pulsed field. Dynamic simulations performed for damping parameters of 0.05 and 0.01 revealed significant ringing of the magnetization components, which was not observed experimentally.

As expected from the experimental data, the ground state magnetization at the center of the element in Fig. 5(a) is rotated 24° from the *x*-axis. The large angle reorientation can be seen clearly in the map of the dynamic magnetization in Fig. 5(b). At the center of the element, the magnetization has reoriented through 92° in good agreement with the experimentally determined value of $100° \pm 10°$. However, it can be seen that the magnetization along the edge parallel to the bias field (*x*-axis) rotates only slightly following the pulsed field excitation. The latter magnetization then acts to return the reoriented moments at the center of the element back to the ground state when the pulsed field is switched off.

In Fig. 5(b) regions of nonuniform magnetization along the edges of the element perpendicular to the bias field are observed. These regions have previously been attributed to regions of small internal field. At sufficiently low bias fields, localized spin wave modes have been observed in the transition region between high internal field at the center of the element and low internal field at the edge of the element.[10,11] The excitation of spin waves has also been suggested as a mechanism for enhanced damping observed for large angle magnetization dynamics.[2] In this work the enhanced damping of the TR Kerr signals may be due to spin wave excitations in the regions of nonuniform magnetization.

In summary we have performed TR measurements of large angle magnetization dynamics in a 2 μm square element with a nonuniform ground state. A large angle reorientation of the magnetization was observed experimentally from a region at the center of the element, in good agreement with micromagnetic simulations. The best agreement was obtained for a damping parameter of 0.1. We suggest that the enhanced damping is a result of the excitation of spin waves in the regions of nonuniform magnetization.

Financial support was provided by the UK Engineering and Physical Sciences Research Council and the New Energy and Industrial Technology Development Organization.

[1] A. Barman, V. V. Kruglyak, R. J. Hicken, J. Scott, A. Kundrotaite, and M. Rahman, J. Appl. Phys. **95**, 6998 (2004).
[2] Th. Gerrits, M. L. Schneider, A. B. Kos, and T. J. Silva, Phys. Rev. B **73**, 094454 (2006).
[3] T. J. Silva, C. S. Lee, T. M. Crawford, and C. T. Rogers, J. Appl. Phys. **85**, 7849 (1999).
[4] Th. Gerrits, H. A. M. van den Berg, J. Hohlfeld, L. Bär, and Th. Rasing, Nature (London) **418**, 509 (2002).
[5] Th. Gerrits, T. J. Silva, J. P. Nibarger, and Th. Rasing, J. Appl. Phys. **96**, 6023 (2004).
[6] A. Krichevsky and M. R. Freeman, J. Appl. Phys. **95**, 6601 (2004).
[7] W. K. Hiebert, G. E. Ballentine, and M. R. Freeman, Phys. Rev. B **65**, 140404(R) (2002).
[8] P. S. Keatley, V. V. Kruglyak, R. J. Hicken, J. R. Childress, and J. A. Katine, J. Magn. Magn. Mater. **306**, 298 (2006).
[9] M. J. Donahue and D. G. Porter, *OOMMF User's Guide, Version 1.0, NISTIR 6376* (National Institute of Standards and Technology, Gaithersburg, MD, 1999): see http://math.nist.gov/oommf.
[10] J. Jorzick, S. O. Demokritov, B. Hillebrands, M. Bailleul, C. Fermon, K. Y. Guslienko, A. N. Slavin, D. V. Berkov, and N. L. Gorn, Phys. Rev. Lett. **88**, 047204 (2002).
[11] C. Bayer, J. Jorzick, B. Hillebrands, S. O. Demokritov, R. Kouba, R. Bozinoski, A. N. Slavin, K. Y. Guslienko, D. V. Berkov, N. L. Gorn, and M. P. Kostylev, Phys. Rev. B **72**, 064427 (2005).